受入
91-8-121
高工研図書室

EUROPEAN ORGANIZATION FOR NUCLEAR RESEARCH

CERN-PPE/91-77
3 April 1991

PROTON DISTRIBUTIONS IN THE TARGET FRAGMENTATION REGION IN PROTON–NUCLEUS AND NUCLEUS–NUCLEUS COLLISIONS AT HIGH ENERGIES

HELIOS Collaboration

T. Åkesson[3], S. Almehed[17], A.L.S. Angelis[20], N.Armenise[1], H. Atherton[3], P. Aubry[8], H.W. Bartels[4], G. Beaudoin[8], J.M. Beaulieu[8], H. Beker[3], O. Benary[18], D. Bettoni[3,a], V. Bisi[19], I. Blevis[21], H. Bøggild[3,b], W. Cleland[12], M. Clemen[12], B. Collick[12], F. Corriveau[7], S. Dagan[18], K. Dederichs[3,c], S. Dell'Uomo[13], P. Depommier[8], R.C.E. Devenish[3,d], S. Di Liberto[13], N. DiGiacomo[5], J.R. Dodd[20], B. Dolgoshein[10], A. Drees[4], H. En'yo[3], B. Erlandsson[17], M.J. Esten[20], C.W. Fabjan[3], P. Fischer[4], Z. Fraenkel[21], A. Gaidot[15], F. Gibrat-Debu[15], P. Giubellino[19], P. Glässel[4], U. Goerlach[4], R. Haglund[6], L.A. Hamel[7], H. van Hecke[5], V. Hedberg[3], R. Heifetz[18], A. Hölscher[4], B. Jacak[5], G. Jarlskog[6], S. Johansson[6], H. Kraner[2], V. Kroh[4], F. Lamarche[7], C. Leroy[7], D. Lissauer[2,18], G. London[15], B. Lörstad[6], A. Lounis[8], F. Martelli[19,22], A. Marzari-Chiesa[19], M.A. Mazzoni[3], E. Mazzucato[7], M.L. McCubbin[20], N.A. McCubbin[14], P. McGaughey[5], F. Meddi[13], U. Mjörnmark[6], M.T. Muciaccia[1], S. Muraviev[9], M. Murray[12], M. Neubert[4], S. Nilsson[17], L. Olsen[2], Y. Oren[18], J.P. Pansart[15], Y.M. Park[12], A. Pfeiffer[4], F. Piuz[3], V. Polychronakos[2], G. Poulard[3], M. Price[3], D. Rahm[2], L. Ramello[19], L. Riccati[19], G. Romano[16], G. Rosa[13], L. Sandor[3], J. Schukraft[3], M. Sekimoto[3,e], B. Sellden[17], M. Seman[3,f], A. Shmeleva[9], V. Sidorov[11], S. Simone[1], Y. Sirois[7], H. Sletten[3], S. Smirnov[10], J. Soltani[4], W. Sondheim[5], H. J. Specht[4], E. Stern[12], I. Stumer[2], J. Sunier[5], V. Tcherniatin[10], H. H. Thodberg[3], J. Thompson[12], V. Tikhomirov[9], I. Tserruya[21], G. Vasseur[15], R. Veenhof[3,g], R. Wigmans[3,g] and P. Yepes[7]

Submitted to Zeitschrift für Physik

See footnotes next page

1) University of Bari and INFN, Bari, Italy
2) Brookhaven National Laboratory, Upton, NY, USA
3) CERN, Geneva, Switzerland
4) Heidelberg University, Fed. Rep. Germany
5) Los Alamos National Laboratory, Los Alamos, NM, USA
6) Lund University, Sweden
7) McGill University, Montreal, Canada
8) University of Montreal, Canada
9) Lebedev Physics Institute, Moscow, USSR
10) Physics Engineering Institute, Moscow, USSR
11) Institute Nuclear Physics, Novosibirsk, USSR
12) University of Pittsburgh, Pittsburgh, PA, USA
13) University of Rome and INFN, Rome, Italy
14) Rutherford Appleton Laboratory, Didcot, UK
15) DPhPE, CEN–Saclay, Gif-sur-Yvette, France
16) University of Salerno and INFN, Salerno, Italy
17) Stockholm University, Sweden
18) Tel Aviv University, Israel
19) University of Turin and INFN, Turin, Italy
20) University College, London, UK
21) Weizmann Institute, Rehovot, Israel
22) Angelo Della Riccia Fellow

Visitors at CERN from:
a) Syracuse University, Syracuse, NY, USA
b) Niels Bohr Institute, Copenhagen, Denmark
c) University of Munich, Fed. Rep. Germany
d) Oxford University, UK
e) Institute of Nuclear Study, Tokyo, Japan
f) Slovak Academy of Sciences, Kosice, Czechoslovakia
g) NIKHEF-H, Amsterdam, The Netherlands

Abstract

We present measurements of the rapidity and transverse-momentum distributions of the protons emitted in S + W, O + W, and p + W reactions at 200 GeV/A around the target rapidity ($y = 1$). The rapidity density rises linearly with the transverse energy for all three systems, but the slope for p + W is much steeper than for O + W and S + W. The rapidity density for p + W is much higher than predicted by summing single nucleon–nucleon collisions without any nuclear effects, indicating substantial rescattering of the produced particles. The predictions of the VENUS 3 model, including rescattering, show reasonable agreement with the data for all three systems. We do not have evidence for a strong collective flow of the outgoing particles.

1 INTRODUCTION

One of the most significant questions to be addressed by experiments on ultrarelativistic heavy-ion collisions is the amount of stopping of the nucleons. This is directly related to the energy and baryon densities early in the collision, and influences a possible deconfinement transition from the hadronic to the partonic phase.

Transverse-energy production at mid and forward rapidities in nucleus–nucleus and p–nucleus collisions [1], [2] is relatively well described by string models, which describe these reactions via a superposition of nucleon–nucleon collisions [3], [4] with slowing between collisions, but without collective effects. At backward rapidities [5]–[7], however, the transverse energy is underestimated in these calculations. This has been attributed to rescattering of the produced secondary particles with the surrounding target matter. This assumption must be tested by comparing the measured baryon distributions in the backward rapidity region with the predicted rescattering effects.

The transverse-momentum distribution of the baryons may be modified by expansion of the participant region, which would add a radial flow component to the emitted particle momenta [8], [9]. Spectra observed for pions have been interpreted in this way [9] and expansion velocities inferred. Owing to the mass difference, comparison of proton transverse momenta with those of pions provides a very sensitive measure of the existence and magnitude of such flow effects.

We present data on proton distributions at rapidities $y = 0.5$–1.5, measured by the HELIOS experiment for 200 GeV per nucleon p, O, and S beams on W targets. We show that the proton distributions in p–nucleus and nucleus–nucleus collisions do not have the same characteristics as in p–p collisions. Rescattering effects are important and the data are consistent with a shift of protons from the target fragmentation region to mid-rapidity. The predictions of several models are examined, and none correctly reproduces all features of the proton distributions. Our data will hopefully allow refinements of the model assumptions about the individual nucleon–nucleon collisions and the rescattering process.

2 EXPERIMENTAL SET-UP

HELIOS has 4π calorimetric coverage with good granularity, which is used to select peripheral and central collisions. The external spectrometer [10], which was used to track and identify the particles, is a magnetic spectrometer covering 15–45° in the laboratory through a narrow azimuthal gap in the calorimeter wall (Fig. 1). It views the target through a horizontal slit covering the pseudorapidity interval $1.0 < \eta < 1.9$. To support the calorimeter, the slit is filled with aluminium hexcell, having a thickness of 3% radiation length. The slit measures 10 cm vertically, varying the azimuthal coverage from 2.1% to 0.75% at the greatest angles from the target.

A magnet with a momentum kick of 80 MeV/c and two high-resolution drift chambers provide the momentum measurement for charged particles. The horizontal coordinate is measured via the drift time ($\sigma_x =\sim 200\,\mu$m) and the vertical coordinate via charge division ($\sigma_y = 0.3$ cm for p + W and S + W and $\sigma_y = 1.0$ cm for O + W). A cut is made on the vertical position of the tracks at the entrance and the exit of the calorimeter wall, which allows elimination of the background from the calorimeters around the slit [10]. The target position is used in the momentum reconstruction, and the effects of multiple scattering are included in the resolution value. The momentum resolution is $\mathrm{d}p/p^2 = 0.08$

for $p \leq 1.0$ GeV/c, and $dp/p = 0.12$ for $p \geq 1.0$ GeV/c up to the highest momenta discussed in this paper [10].

Particles are identified using two time-of-flight scintillator hodoscopes behind the second drift chamber. The flight path from the target is 5 m. The first wall covers the small-angle section of the acceptance, and has a time resolution $\sigma_t = 250$ ps. It is composed of 9 cm × 15 cm paddles. This hodoscope was used in the p + W and S + W runs to separate kaons, pions, and protons. The time resolution of the second wall is about 550 ps, which is adequate to resolve protons and pions at the large angles and relatively low momenta (< 1.5 GeV/c) prevalent in the backward part of the spectrometer. The second wall also provides a redundant measurement in the forward part of the spectrometer. It consists of two rows of square counters. These measure 10 cm × 10 cm at the small angles and 15 cm × 15 cm at larger angles. The efficiency loss arising from the small dead area between counters is corrected via Monte Carlo simulations. In the O + W runs only the second (550 ps) wall was used.

The trigger for these data required a valid interaction of the beam, determined by a minimum multiplicity in silicon counters immediately downstream of the target, and also used the transverse energy measured in the calorimeters in the pseudorapidity range $-0.1 < \eta < 2.9$. Varying scale-down factors for different E_t thresholds were used, providing similar statistics across the E_t range, effectively sampling a wide range of impact parameters [5]. To enrich the minimum-bias event sample, a trigger requiring hits in the spectrometer time-of-flight (TOF) counters was used. Tungsten disk targets were used for the data presented in this paper.

3 DATA ANALYSIS AND MONTE CARLO CORRECTIONS

Track-reconstruction is carried out by matching the track segments from each drift chamber and fitting these, along with the target position [10]. The mean number of tracks per event ranges from less than one for p + W collisions, to 1.6 for S + W collisions. Particles are identified by calculating the mass from the momentum determined by the tracking procedure and the flight time measured in the scintillator walls. The TOF counters were calibrated using pions between 0.6 and 1.2 GeV/c, where they are unambiguously separated from other particles. For these pions, the measured TOF was compared with the expected time for the path through the spectrometer, extrapolating the drift-chamber tracks to the target and the scintillator wall. The calibrations were verified using negative particles with $p > 1.8$ GeV/c. Their velocity was assumed to be the speed of light; as these are predominantly pions, this is true to within a fraction of 1%.

To separate the protons from pions and kaons, the particles are sorted into narrow ranges of momentum, and the square of the mass, m^2, is calculated. The m^2 distribution for S + W for a large momentum range is shown in Fig. 2. Cuts on m^2 are used to identify the protons; these cuts have a very small variation with momentum. Any errors in calibration, such as the assumed velocity of the calibration particles and uncertainties in the flight path which would affect the calculated mass, are taken into account by the choice of the cuts.

The external spectrometer has a fixed acceptance in pseudorapidity, so the proton rapidity acceptance depends on p_t; this dependence is shown in Fig. 3. Consequently the proton distributions are analysed as a function of both rapidity and transverse momentum. These distributions are corrected by a Monte Carlo simulation of various detector effects, including the spectrometer acceptance, track-reconstruction efficiency, momentum

resolution, efficiency of matching tracks to the scintillators, scintillator efficiencies, and TOF resolution. This procedure also simulates the effects of multiple scattering and energy loss of the protons. Protons are generated using a flat rapidity distribution, and a p_t distribution based on a parameterization of proton p_t spectra from the CERN ISR p–p measurements [11]. The geometry and response of the various detectors is simulated, tuning the resolutions to those observed in the data. These simulated events are then reconstructed using the full analysis chain, and the ratio of generated input to reconstructed Monte Carlo spectra is used to correct the data.

The number of protons per event is normalized by choosing a window in p_t and rapidity well inside the spectrometer acceptance, and counting protons found in events within certain ranges of E_t. The number of protons is corrected via Monte Carlo for tracking and identification inefficiencies, and normalized by the total number of events recorded in the relevant E_t range.

4 SYSTEMATIC ERRORS

The systematic error in the p_t distributions is dominated by the momentum resolution. The uncertainty in the cross-sections at $p_t = 1$ GeV/c is 3% [10]. The systematic error on the rapidity distributions is also dominated by the momentum resolution. The systematic error on the angle measurement arises from multiple scattering and is 3–4% at low momenta (< 0.5 GeV/c) and 0.5–1% at high momenta.

Misidentification of particles by the mass cuts may result in the loss of protons outside the cuts, or pions and kaons being erroneously counted as protons. These effects have been corrected via Monte Carlo, but systematic errors arise because the data and Monte Carlo distributions are not identical. The r.m.s. widths of the m^2 distributions in the data are 0.1–0.25 GeV$^2/c^4$, whilst the Monte Carlo distributions are narrower by 20–25%. However, the m^2 gates are 1.12 GeV$^2/c^4$ wide, approximately 4.5σ at high momentum. Consequently, the correction for proton losses is small. The systematic error in the correction for proton losses arises from the difference in width between Monte Carlo and data and is approximately 2%. The contamination of protons by π and K was estimated by studying the negative particle data. For p + W, this contamination is negligible below $p = 0.8$ GeV/c. The contamination is 0.3% at $p = 0.8$ GeV/c, and rises to 1.5% at 1.8–2 GeV/c. For O + W and S + W, the higher ratio of pions and kaons to protons results in a larger contribution of the π and K tails misidentified as protons; the contamination at the highest momenta is 3% for S + W and 8% for O + W. The rapidity distributions are not affected by contamination at these levels, and the p_t distributions do not show systematic changes either. Consequently, corrections for contamination effects have not been made. A study was made to check for E_t dependence of contamination effects on the p_t slopes; within the 6% statistical accuracy of the study, no E_t dependence was observed.

The size of pile-up effect in the TOF counters was determined from the average occupancy of the individual TOF modules and was checked by mixing tracks and scintillator hits from different events, and looking for protons lost owing to the calculation of an incorrect mass. Pile-up effects were found to be approximately 1% for all p + W events. For S + W, the pile-up is 2% at low E_t, and rises to 3% in high-E_t events. The pile-up effect is concentrated at small angles, reaching 4% at the smallest angles and falling below 1% for $\theta \geq 25$–$30°$. Because of the larger area of the individual TOF scintillators used in the O + W experiment the pile-up effect was considerably larger. It increases from 1%

at $\eta = 1.0$ to 9% at $\eta = 1.8$. The O + W data have been corrected for this effect. The systematic error due to pile-up is estimated to be 5%.

Variations in the scintillator efficiencies create a 5% systematic uncertainty in the absolute number of protons. This effect should be considerably smaller in the rapidity and p_t distributions owing to the spreading of the protons across the spectrometer.

The overall systematic error for dN/dy in S + W and O + W collisions is estimated to be 6.3% and 9% respectively.

5 RESULTS

Figure 4 shows the rapidity distribution of protons from S + W collisions at low and high E_t (E_t in the region $-0.1 < \eta < 2.9$), corresponding to peripheral and central collisions. The curves shown correspond to five bins in the p_t spectrum. The rapidity distributions are relatively flat, falling off less steeply than those observed in p–p collisions at the same $\sqrt{s}$ [11]. For $p_t > 0.6$ GeV/c, the rapidity distribution is flatter than at lower p_t, and even appears to rise slightly. No significant difference in the shape of the proton rapidity distributions is observed as a function of E_t.

Figure 5 shows the proton rapidity distributions for O + W collisions for the same p_t bins, for $15 < E_t < 100$ GeV and $E_t > 100$ GeV. Whilst the distributions show the same general trend as those of S + W, the slopes of O + W are considerably steeper. We shall return to this point below.

Figure 6 shows the proton rapidity distributions from p + W collisions for both minimum-bias and high-E_t events. Although fewer protons are observed in p + W than in O + W and S + W collisions, the shape of the rapidity distribution is not very different within the statistical errors of our measurement. As in O + W and S + W collisions, the trend does not change with E_t.

Although the shape of the proton rapidity distributions is remarkably independent of E_t, the number of protons observed in our acceptance rises with E_t for all projectiles. Figure 7 shows the rapidity density of protons as a function of E_t for p + W, O + W, and S + W. The right-hand scale gives the rapidity densities measured in the external spectrometer, whilst the left-hand scale shows values extrapolated over the entire p_t spectrum. This extrapolation was made using the FRITIOF event generator [2], since the predicted proton p_t distributions agree reasonably well with the data above $y = 0.5$. The results are plotted as a function of the measured E_t value, but the E_t distribution reaches much larger values for ion projectiles than for protons. The 'knee' of the S + W E_t distribution, where the projectile and target fully overlap in a simple geometrical picture, is at $E_t \sim$ 200 GeV. However, $E_t = 30$–40 GeV is far down in the tail of the p + W E_t distribution. The number of protons rises approximately linearly with E_t for all three projectiles.

Toothacker et al. [12] report the proton rapidity density from minimum-bias collisions of 100 GeV p + Ag to be peaked at $y_{\mathrm{lab}} = 0$ with $dN/dy = 5$, and $dN/dy = 0.8$ at $y = 1$. They find that the number of target rapidity protons increases with the rapidity loss of the leading baryon. We find 5.7 protons per unit rapidity at $y = 1$ in high-E_t p + W collisions. Central O + W and S + W, corresponding to $E_t = 120$ and 200 GeV, produce proton rapidity densities, at $y = 1$, of 12.5 and 17 respectively.

The proton p_t distributions for S + W and p + W are presented in Figs. 8 and 9. Figure 8 shows the distributions for low-E_t (peripheral) and high-E_t (central) S + W collisions. Figure 9 shows the distributions for minimum-bias and high-E_t p + W collisions. Each data set includes several curves corresponding to the distributions in

various regions of rapidity from $y = 0.4$ to 1.4. The solid lines indicate the proton p_t distributions observed at central rapidity in p–p collisions at $\sqrt{s} = 23$ GeV [11]. For $y > 0.5$, p–nucleus and low-E_t nucleus–nucleus proton p_t distributions have the same slope as p–p collisions.

Figure 10 summarizes the rapidity dependence of the inverse slopes of the observed proton p_t distributions, and also shows their E_t dependence. Figure 10a shows the results from S + W; the slopes depend somewhat on rapidity, but increase with larger E_t. A similar trend is seen in Fig. 10b for the results from O + W. In Fig. 10c, the p + W spectra have a larger increase in slope with increasing rapidity, but show a smaller dependence on the E_t of the event. Peripheral O + W and S + W collisions produce proton p_t slopes comparable with those in p + W. Central O + W and S + W collisions produce flatter proton p_t distributions than p–p or p + W; a similar result was observed at $y = 0.2$ for O + Au collisions [13] by the WA80 Collaboration.

Figure 11 shows the dependence of the slope of the proton p_t distribution on E_t in S + W and O + W collisions. The slope increases with E_t, up to very central collisions. This behaviour is qualitatively different from that of the pions [10], where the slope increases with E_t (to $E_t \approx 75$ GeV for S + W and $E_t \approx 50$ GeV for O + W) and then stays constant with further increases in E_t.

In order to determine the rapidity density of antiprotons in the S + W data sample, mass spectra for positive and negative particles were accumulated in the interval $y = 0.6$–1.2 and $p_t = 0.3$–0.75. The positive spectrum shows peaks for pions, kaons, and protons, whilst the negative spectrum is dominated by pions and kaons only. The contribution of pions and kaons is subtracted by fitting the pion and kaon mass peaks and subtracting the fit from the spectrum as a whole. The residual spectrum should then be dominated by the antiprotons. Although this method is very sensitive to the systematics of the kaon fit, we have derived an upper limit for antiproton production by carefully fitting the observed pion and kaon peak shapes. Following the π/K subtraction, an estimate of the random background was made from the mass region 1.4–1.9 GeV for negative particles. Performing the same procedure on the positive particles should result in a cancellation of most systematic errors. The upper limit for $\bar{p}/p$ was found to be 0.8%, at the 95% confidence limit.

6 DISCUSSION

In order to understand the rapidity distribution of protons observed in both p–nucleus and nucleus–nucleus collisions, we have used several Monte Carlo event generators.

FRITIOF [3] is a string model which treats the collisions as a superposition of nucleon–nucleon interactions; the nucleons lose energy between collisions, but otherwise the collisions are independent. The strings thus formed fragment independently; the fragmentation is known phenomenologically from e^+e^- collisions. FRITIOF is the extension to nucleus–nucleus collisions of the LUND model [14], which reproduces the charged-particle distributions observed in p–p collisions. Protons produced by FRITIOF arise primarily from the fragmentation of participating projectile and target nucleons. Rescattering of produced particles and fragmentation products in the target is not addressed by FRITIOF, but may strongly influence the observed proton distributions, particularly at target rapidities. It is also likely that the projectile nucleons are stopped more efficiently by nuclear targets than by proton targets.

A second string model has been proposed by Werner [15], [16]. In this model, VENUS 3, the string formation is based on the principles of the Dual Parton Model [4], but non-diffractive collisions are allowed between nucleons at any stage in the event. VENUS includes colour exchange between antiquarks as well as between quarks. VENUS 3 also includes the reinteraction of decay products from string fragmentation among themselves and with spectator nucleons [16]. Consequently, we use VENUS 3 to study both increased stopping and reinteraction effects on the proton distributions.

Figure 12 shows the proton rapidity distributions predicted for central collisions of S + W ($E_t > 180$ GeV) and O + W ($E_t > 130$ GeV), and high-E_t ($E_t > 18$ GeV) p + W collisions by FRITIOF and by VENUS 3 with and without reinteractions of produced particles. The models are compared with one another, as well as with the data. The crosses indicate the measured proton rapidity densities, corrected for acceptance effects in p_t as described above. The simulated events were selected by scaling the E_t distributions for $-0.1 < \eta < 2.9$ from the models to agree with the measured E_t spectrum and applying the same E_t selection as for the external spectrometer data. (This is done so that the comparison is made for approximately the same range of impact parameters.)

For p + W, VENUS 3 without reinteractions produces similar rapidity densitites to FRITIOF at $y = 1$, but the protons are produced over a somewhat broader rapidity interval. Reinteractions increase sharply the number of protons produced near target rapidity. Comparison of the data with the generators shows production of more protons in high-E_t events than predicted either by FRITIOF or by VENUS 3 without reinteractions. The importance of rescattering on the number of protons observed is clearly indicated.

For central O + W and S + W collisions, VENUS 3 without reinteractions predicts a peak in the proton rapidity distribution which is broader and centred at higher rapidity than the FRITIOF predictions. Comparing the two versions of VENUS 3 shows that the rescattering again increases the number of protons observed at target rapidity ($y \leq 1.5$), and also shifts a few protons from mid-rapidity to lower y. Equally significant is the fact that the second peak in the rapidity distribution in S + W (and perhaps also in O + W) at $y \approx 4.5$ predicted by FRITIOF, is completely absent in that predicted by VENUS; this second peak close to the beam rapidity peak is indicative of projectile nucleons completely traversing the target nucleus with relatively little loss in momentum. Both features indicate that even without reinteractions VENUS predicts substantially more stopping than FRITIOF. We also see that VENUS with reinteractions correctly reproduces the steeper drop of the rapidity distribution in the range $0 < y < 1$ for O + W (Fig. 5) as compared with S + W (Fig. 4). Since this feature is not seen in VENUS without interactions and FRITIOF, we may conclude that it is the result of secondary reinteractions in the target nucleus.

Because of the limited range (in y) of the experimental rapidity distributions and the fact that none of the models accurately reproduces the experimental points, it is difficult to conclude that any of the three models fits the experimental results based on the rapidity distributions alone. However, VENUS with reinteractions seems to predict more closely the trend of the experimental data for p + W as well as for O + W and S + W, whereas VENUS without reinteractions clearly underestimates the rapidity distribution in target rapidity region for all three experimental systems. A detailed comparison of the predictions of the three models with the experimental rapidity and transverse-momentum distributions shows that VENUS with reinteractions generally agrees best with the experimental data. Figure 11 compares the slopes of the proton p_t distribution as a function of

E_t in the data and the three models for O + W [19]. VENUS with reinteractions describes the data fairly well. For p + W and S + W collisions, the agreement is not as good as for O + W, but the general trends of the data are reproduced.

The possibility of a collective flow of the expanding fireball can be addressed by our data in a comparison of the p_t spectra of pions and protons. A high flow velocity would produce on average transverse momenta of protons substantially larger than the pion $\langle p_t \rangle$. Jacak [17] compared the p_t spectra of π, K, protons, and Λ particles in S + Au and S + S collisions at 200 GeV/A [18] and found that these spectra have approximately the same slope as a function of transverse mass, $m_t = \sqrt{m^2 + p_t^2}$. Such behaviour can be expected from a thermal distribution, but the scaling in slope should be broken by collective flow [17]. The same characteristics are found for the protons discussed in the present paper as those for the negative particles [10] (predominantly pions) measured in the same spectrometer, again providing no compelling evidence for a sizeable collective flow. We can also look for a flow effect by comparing the characteristics of the experimental p_t spectra with the predictions of theoretical models. We have shown in Fig. 11 that the slopes of the proton p_t spectra rise with the transverse energy E_t, but the pions do not show an identical effect [10]. FRITIOF and VENUS without reinteractions show no E_t dependence of either pion or proton p_t distributions. Introducing rescattering into VENUS causes the proton slopes to increase with E_t, qualitatively reproducing the data. As VENUS does not include collective flow, this result indicates that the E_t dependence of the proton slopes is probably a rescattering effect rather than due to collective flow. We note, however, that collective flow effects are expected to be strongest in the mid-rapidity region, and the rapidities examined in the present experiment are one to two units below mid-rapidity.

7 CONCLUSIONS

We have measured the proton rapidity densities and transverse-momentum distributions around rapidity $y = 1$ for E_t selected p + W, O + W and S + W collisions. The data show a flatter dN/dy and higher baryon rapidity density near the target than expected from a simple superposition of nucleon–nucleon collisions. The values are more consistent with expectations from models that include reinteractions of produced particles and spectator matter, as well as a considerable amount of stopping.

The p_t distributions for protons at $y > 0.5$ look like those observed in p–p collisions for both p + W and peripheral O + W and S + W events. Below $y = 0.5$, the distributions are steeper. A dependence of the slopes on E_t is observed; this dependence is very small in p + W collisions, but the proton p_t spectra become flatter with increasing E_t in O + W and S + W. Whilst currently available models do not fully explain the data, VENUS 3 with secondary interactions of the produced particles includes the essential physics of these collisions, at least in the rapidity range of the present investigation.

Acknowledgements

The HELIOS Collaboration acknowledges the outstanding performance of the PS–SPS accelerator complex. We thank the staff of the GSI Computer Center for providing resources and help in the data analysis. We appreciate discussions with G. Baym, H. Heiselberg, and Klaus Werner whom we wish to thank for making the VENUS 3 code available to us. We are grateful for support by the Natural Science and Engineering Research Council of Canada, the Institut de Recherche Fondamentale (CEA, France),

the German Federal Minister for Research and Technology, the U.S.–Israel Binational Science Foundation, the Istituto Nazionale di Fisica Nucleare of Italy, the Science Research Council of the United Kingdom, and the US Department of Energy.

REFERENCES

[1] A. Bamberger et al., NA35 Collaboration, Phys. Lett. **B205**, 583 (1988).
[2] R. Albrecht et al., WA80 Collaboration, Phys. Lett. **B199**, 297 (1987).
[3] B. Anderson, G. Gustafson, and B. Nielsson-Almqvist, Nucl. Phys. **B281**, 289 (1987).
[4] A. Capella and J. Tran Thanh Van, Phys. Lett. **93B**, 146 (1980).
[5] T. Åkesson et al., HELIOS Collaboration, Z. Phys. **C38**, 383 (19988);
T. Åkesson et al., HELIOS Collaboration, Phys. Lett. **B214**, 295 (1988);
[6] J. Schukraft, Z. Phys. **C38**, 59 (1988).
G. London, HELIOS Collaboration, Proc. Europhysics Conf., Madrid, Spain, Sept. 1989.
[7] J.P. Pansart, Nucl. Phys. **A461**, 521c (1987).
[8] M. Kataja, P.V. Ruuskanen, L. McLerran and H. von Gersdorff, Phys. Rev. **D34**, 2755 (1986).
[9] K.S. Lee and U. Heinz, Z. Phys. **C43**, 425 (1989).
[10] T. Åkesson et al., HELIOS Collaboration, Z. Phys. **C46**, 361 (1990).
[11] B. Alper et al., Nucl. Phys. **B100**, 237 (1975).
[12] W.S. Toothacker et al., Phys. Lett. **B197**, 295 (1987).
[13] R. Albrecht et al., WA80 Collaboration, Z. Phys. **C45**, 529 (1990).
[14] B. Anderson, G. Gustafson and C. Peterson, Phys. Lett. **B69**, 221 (1977) and **B71**, 337 (1977).
[15] K. Werner, Phys. Rev. Lett. **62**, 2460 (1989).
[16] K. Werner and P. Koch, Phys. Lett. **B242**, 251 (1990) and Phys. Rev. **C24**, 488 (1981).
[17] B. Jacak, to be published in Proc. Quark Matter '90 Conference, Menton, France, 1990.
[18] J.W. Harris, Nucl. Phys. **A498**, 133c (1989).
[19] I. Blevis, Ph.D. Thesis, Weizmann Institute, 1991, unpublished.

Figure captions

Fig. 1: Schematic diagram of the external spectrometer of the HELIOS experiment.

Fig. 2: Calculated mass-squared distribution for positive particles. The truncated peak consists of pions; the smaller peaks indicate kaons and protons.

Fig. 3: Acceptance plot for protons as a function of rapidity and p_t. The lines labelled 15° and 45° bracket the spectrometer acceptance, whilst the intersecting lines indicate the proton momentum at given y and p_t.

Fig. 4: dN/dy for protons from S + W collisions. Events are sorted according to the transverse energy measured in the HELIOS calorimeters. The upper section corresponds to low E_t, or peripheral collisions, and the lower section to high E_t, or central collisions. The separate curves indicate protons within different regions of p_t; the lines are to guide the eye.

Fig. 5: The same as Fig. 4, but for O + W collisions. Note that the upper section contains low- and medium-E_t events, corresponding to a larger range of impact parameters than the upper section of Fig. 4.

Fig. 6: dN/dy for protons from p + W collisions. The upper section represents minimum-bias events, and the lower section shows distributions from high-E_t events.

Fig. 7: dN/dy for protons as a function of transverse energy for p + W, O + W, and S + W collisions. The protons are counted in the rapidity region $0.7 < y < 1.0$, and the scale on the right indicates the rapidity density for the limited p_t range accessible in the external spectrometer. The left-hand scale results when the measured p_t distributions are extrapolated to all p_t using FRITIOF.

Fig. 8: Distributions dN/dp_t^2 plotted against p_t for protons from S + W collisions. The left side of the figure shows the distributions from low-E_t events, and the right that from high-E_t events. The different curves indicate protons in various ranges of rapidity. The solid lines show the slope of proton p_t distributions in the central region of p–p collisions at the same $\sqrt{s}$ [11].

Fig. 9: The same as Fig. 8, but for protons from p + W collisions.

Fig. 10: The dependence of the slopes of proton p_t distributions on the rapidity. Results for the three systems are shown for a number of E_t ranges.

Fig. 11: Dependence of the slope of the proton p_t spectra on the transverse energy for O + W and S + W collisions. The rapidity interval is $0.5 < y < 1.1$ for O + W and $0.75 < y < 1.0$ for S + W. Also shown are the predictions of FRITIOF (dashed line), VENUS without rescattering (solid line), and VENUS with rescattering (dotted line) for O + W in the same rapidity interval. The experimental data are indicated by the solid points.

Fig. 12: Comparison of the proton rapidity densities from three different models with the data for high-E_t S + W, O + W, and p + W collisions. The dashed line shows the predictions of the FRITIOF model, the solid line shows the predictions of VENUS 3 without rescattering, and the dotted line the predictions of VENUS 3 including rescattering in the target. The data are indicated by the crosses.

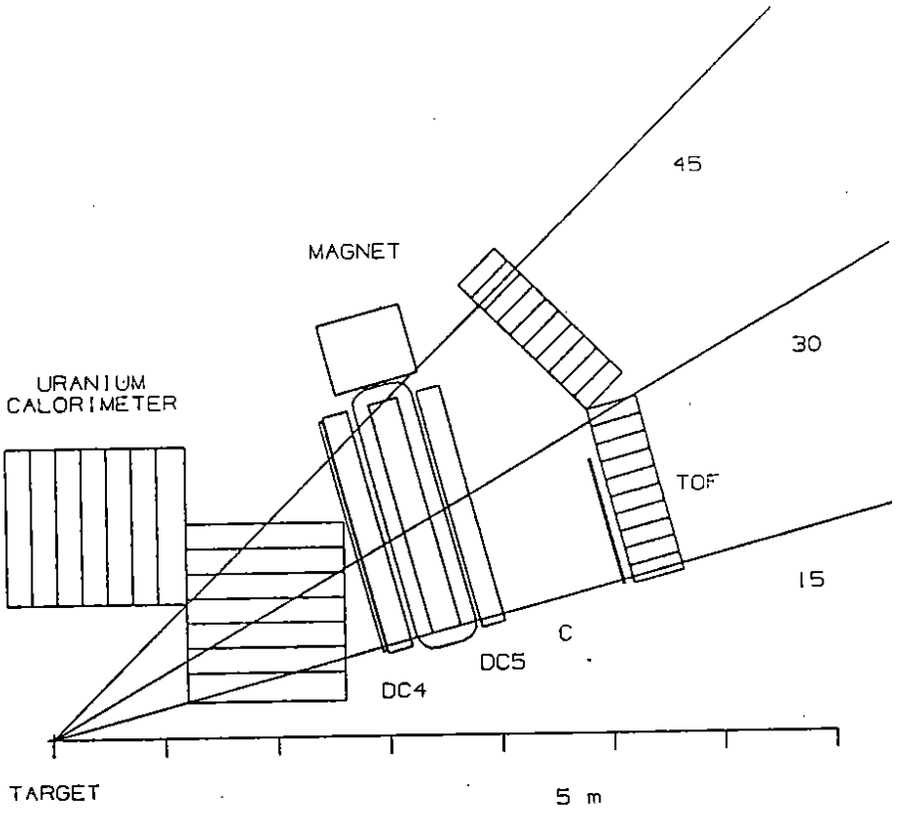
45
MAGNET
30
URANIUM
CALORIMETER
TOF
15
C
DC5
DC4
TARGET
5 m

Fig. 1

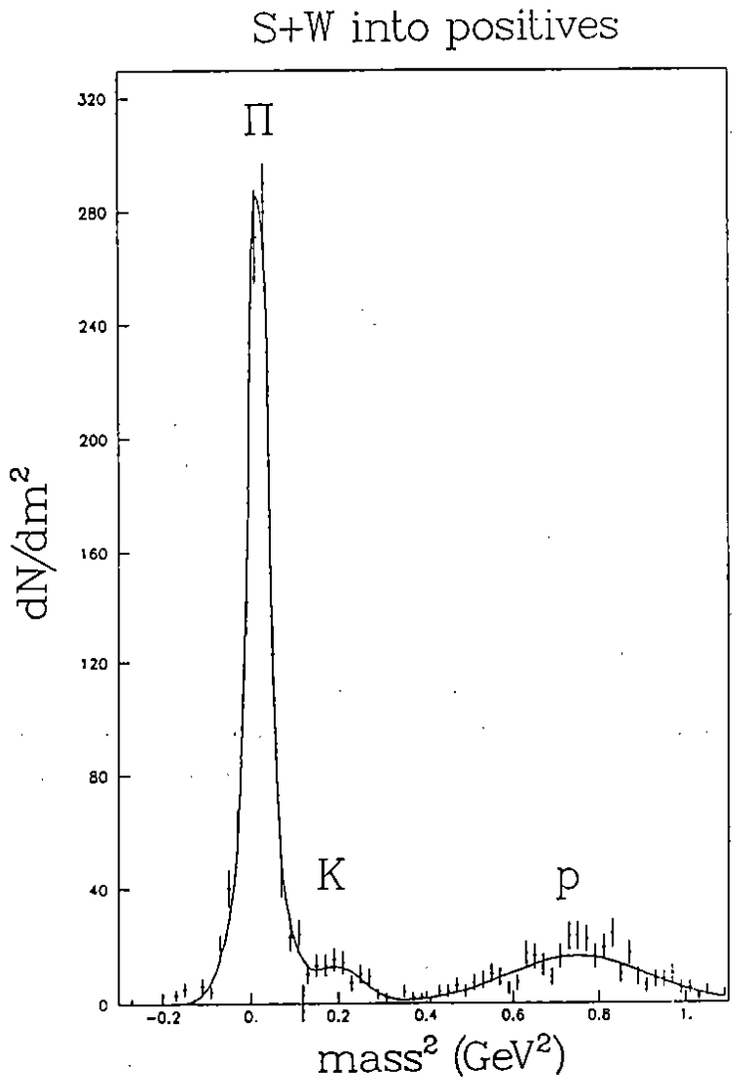
S+W into positives
Π
K
p
dN/dm²
mass² (GeV²)
320
280
240
200
160
120
80
40
0
-0.2
0.
0.2
0.4
0.6
0.8
1.

Fig. 2

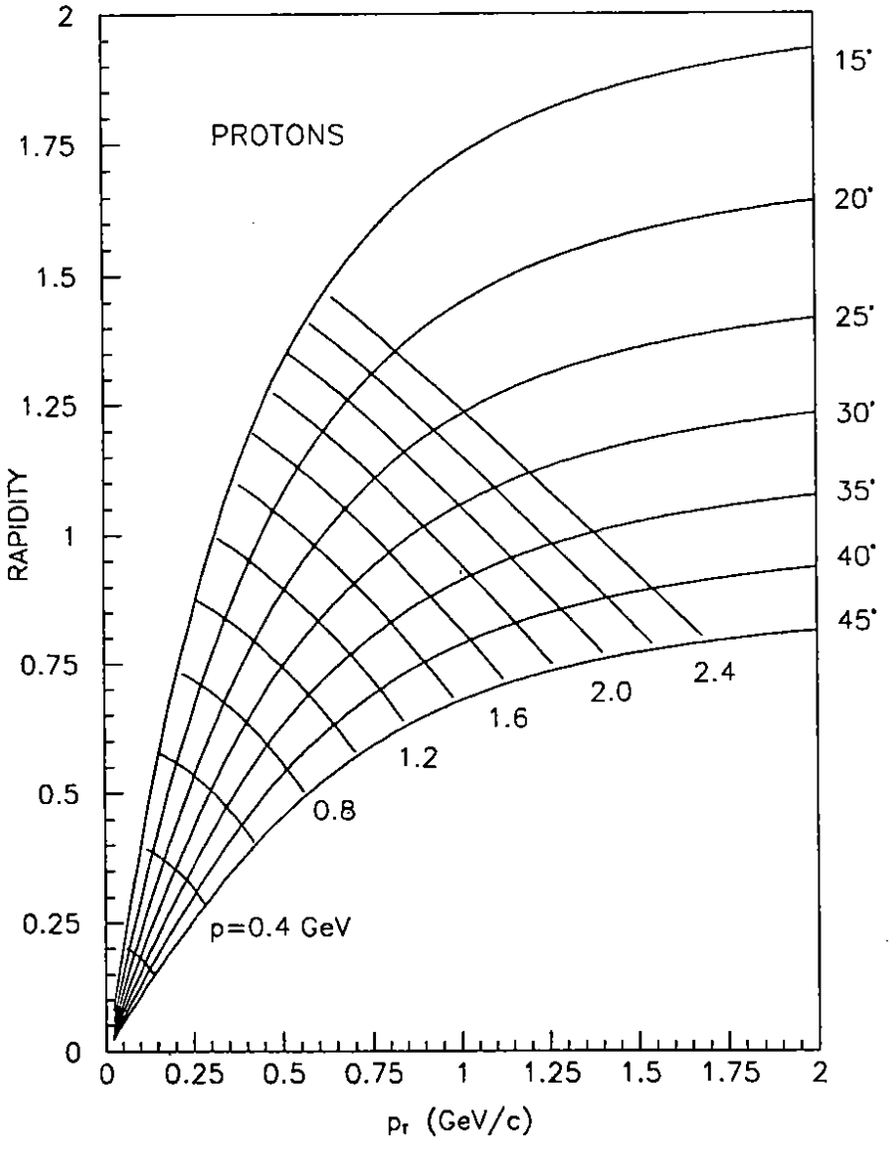
PROTONS
RAPIDITY
p_T (GeV/c)
p=0.4 GeV
0.8
1.2
1.6
2.0
2.4
15°
20°
25°
30°
35°
40°
45°

Fig. 3

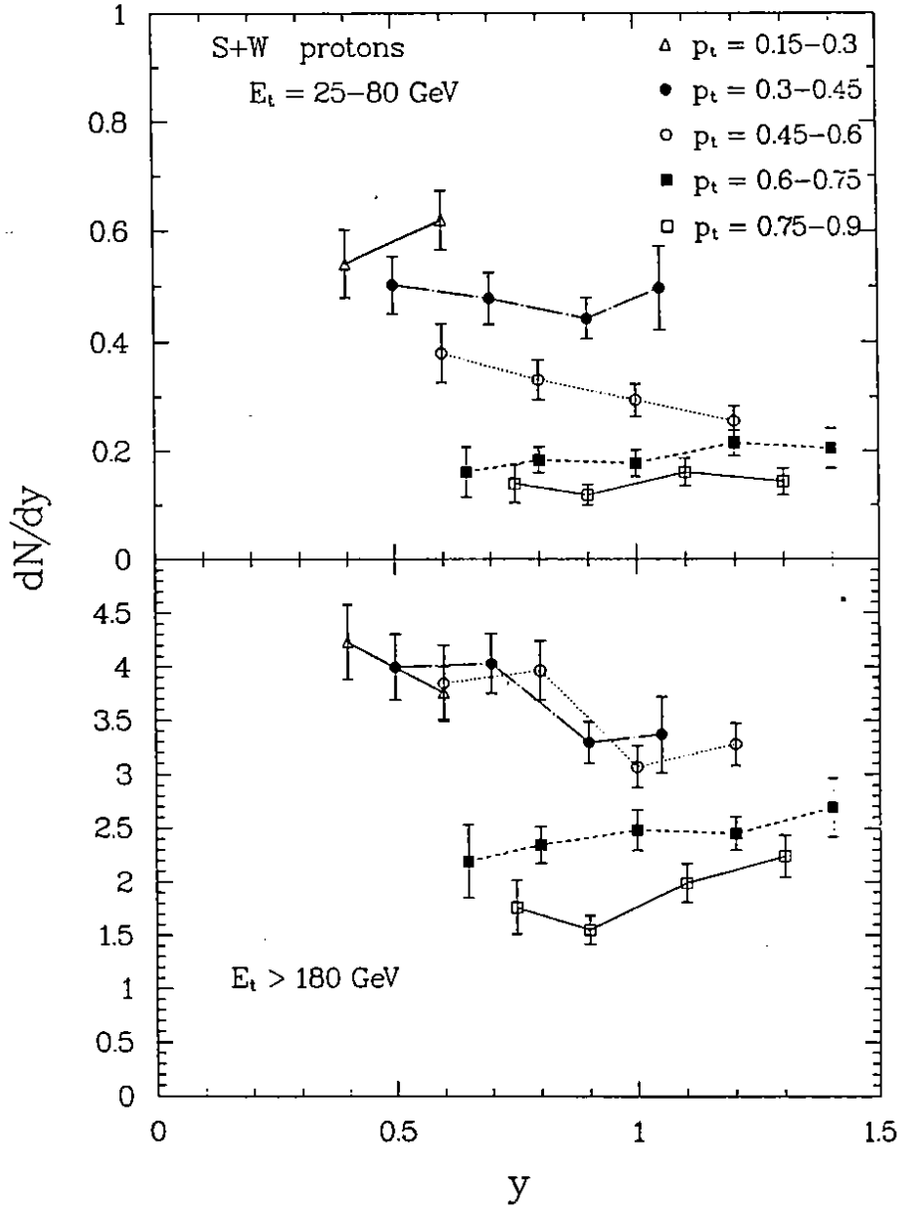
S+W protons
E_t = 25–80 GeV
p_t = 0.15–0.3
p_t = 0.3–0.45
p_t = 0.45–0.6
p_t = 0.6–0.75
p_t = 0.75–0.9
E_t > 180 GeV
dN/dy
y

Fig. 4

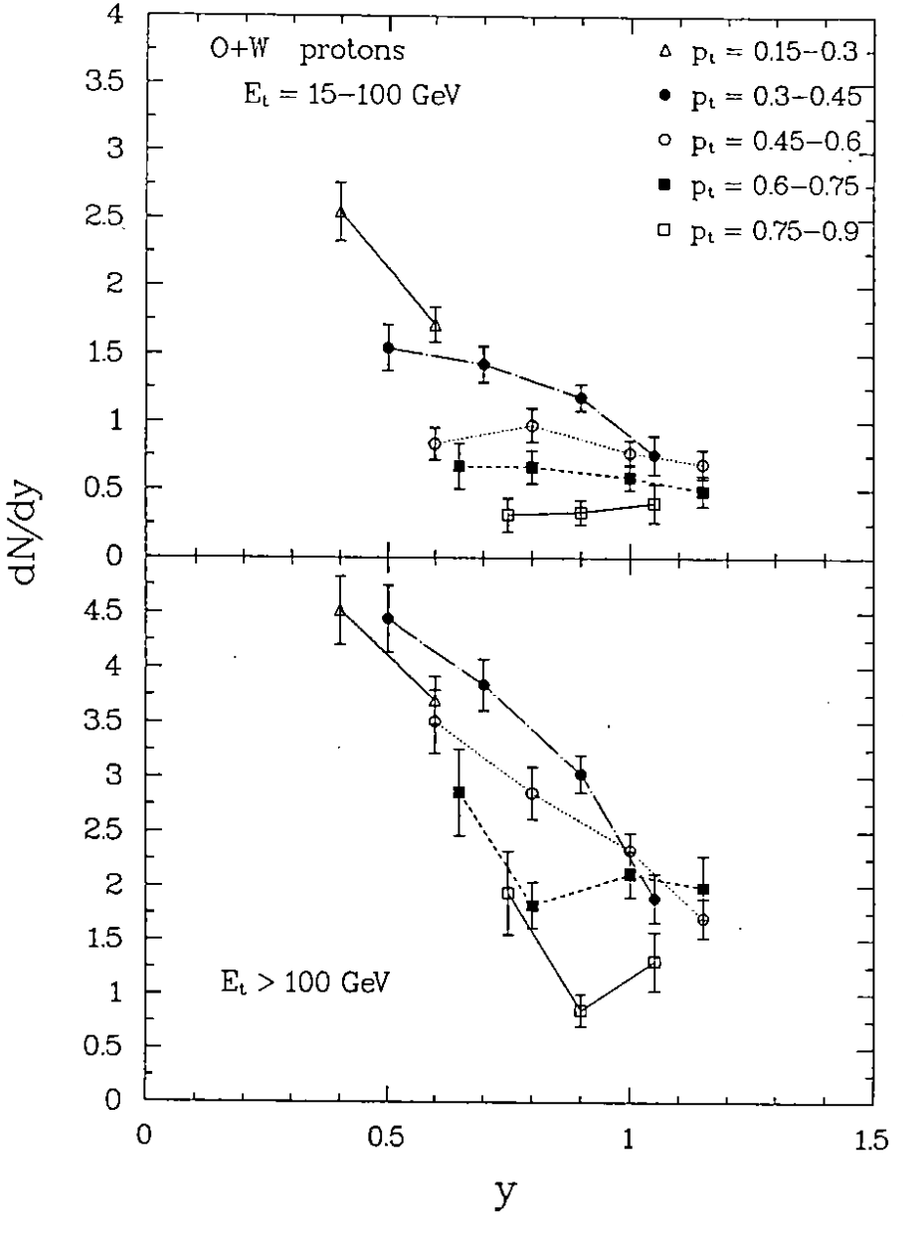
O+W protons
E_t = 15–100 GeV
p_t = 0.15–0.3
p_t = 0.3–0.45
p_t = 0.45–0.6
p_t = 0.6–0.75
p_t = 0.75–0.9
E_t > 100 GeV
dN/dy
y

Fig. 5

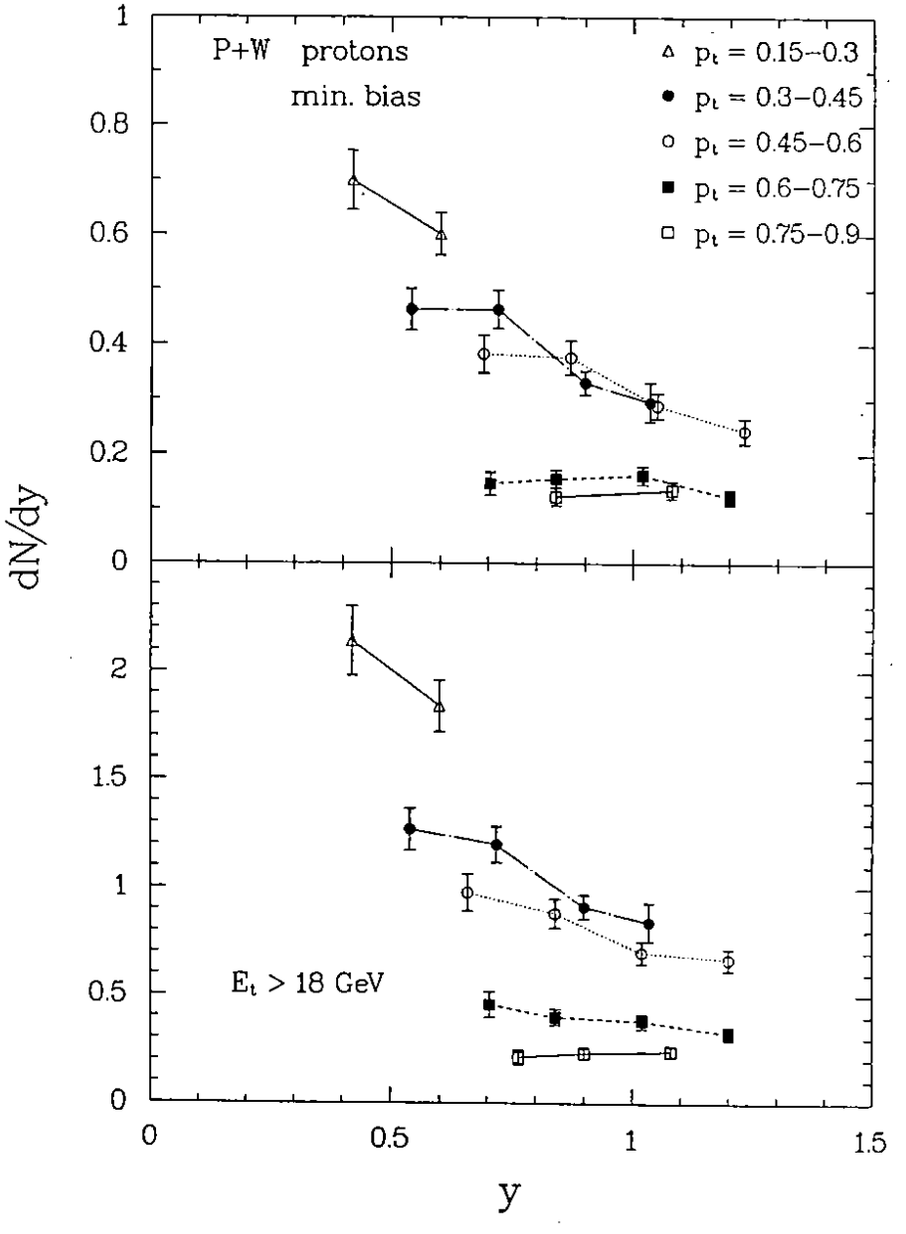
P+W protons
min. bias
p_t = 0.15–0.3
p_t = 0.3–0.45
p_t = 0.45–0.6
p_t = 0.6–0.75
p_t = 0.75–0.9
E_t > 18 GeV
dN/dy
y

Fig. 6

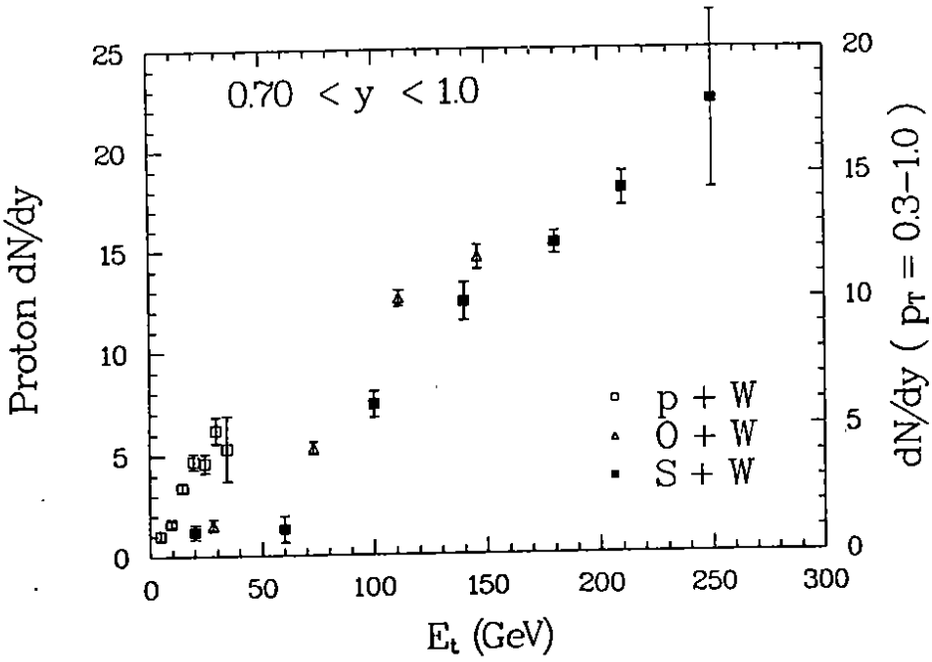
0.70 < y < 1.0
p + W
O + W
S + W
Proton dN/dy
dN/dy (p_T = 0.3–1.0)
E_t (GeV)

Fig. 7

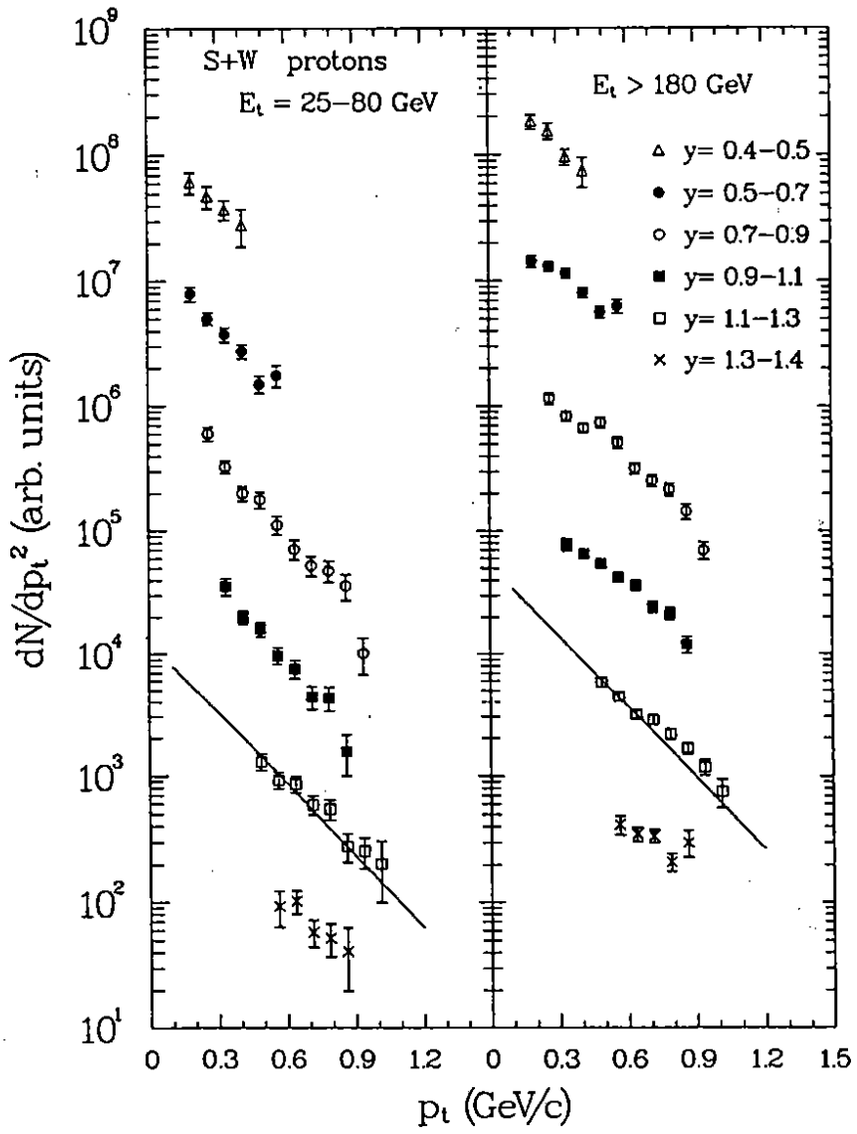
S+W protons
E_t = 25–80 GeV
E_t > 180 GeV
y= 0.4–0.5
y= 0.5–0.7
y= 0.7–0.9
y= 0.9–1.1
y= 1.1–1.3
y= 1.3–1.4
dN/dp_t^2 (arb. units)
p_t (GeV/c)

Fig. 8

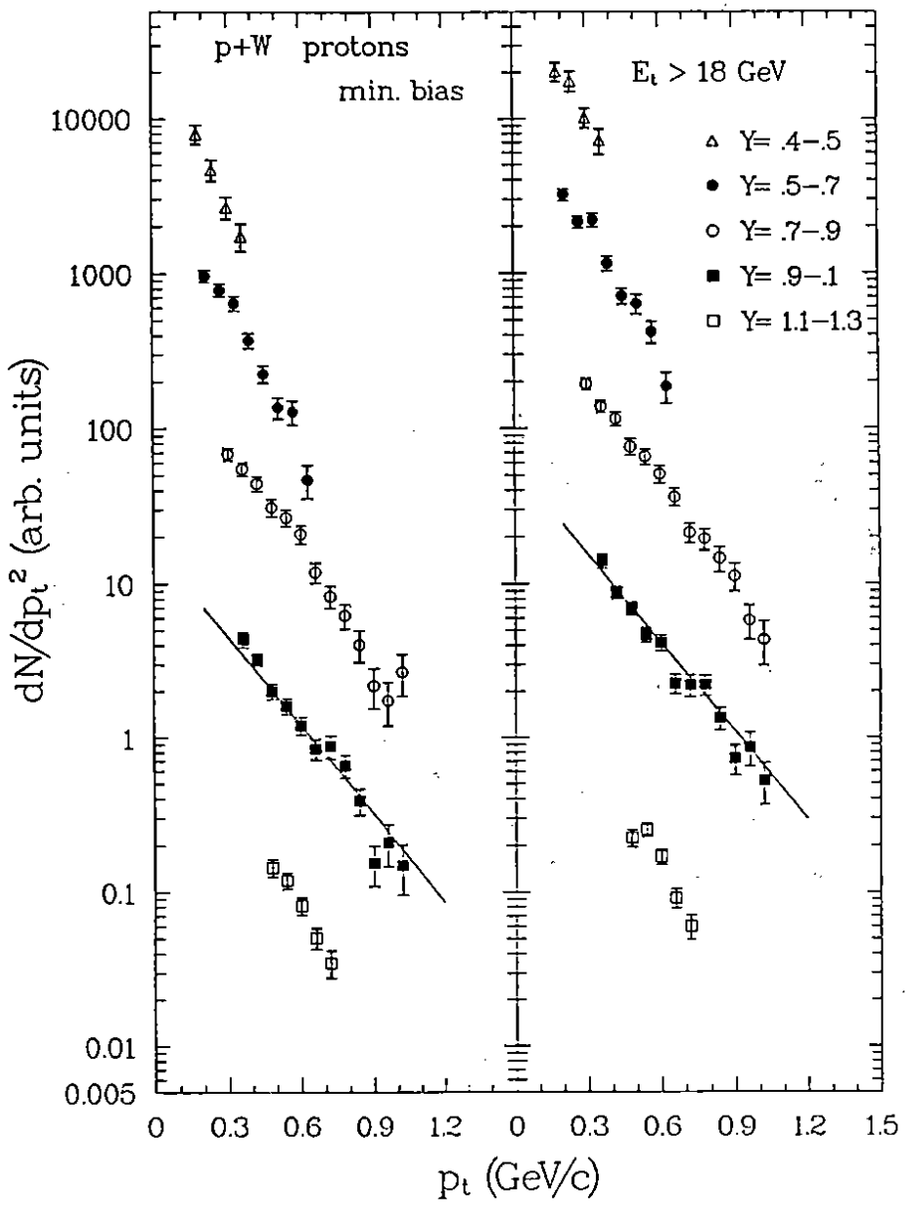
p+W protons
min. bias
E_t > 18 GeV
Y= .4–.5
Y= .5–.7
Y= .7–.9
Y= .9–1.1
Y= 1.1–1.3
dN/dp_t^2 (arb. units)
p_t (GeV/c)

Fig. 9

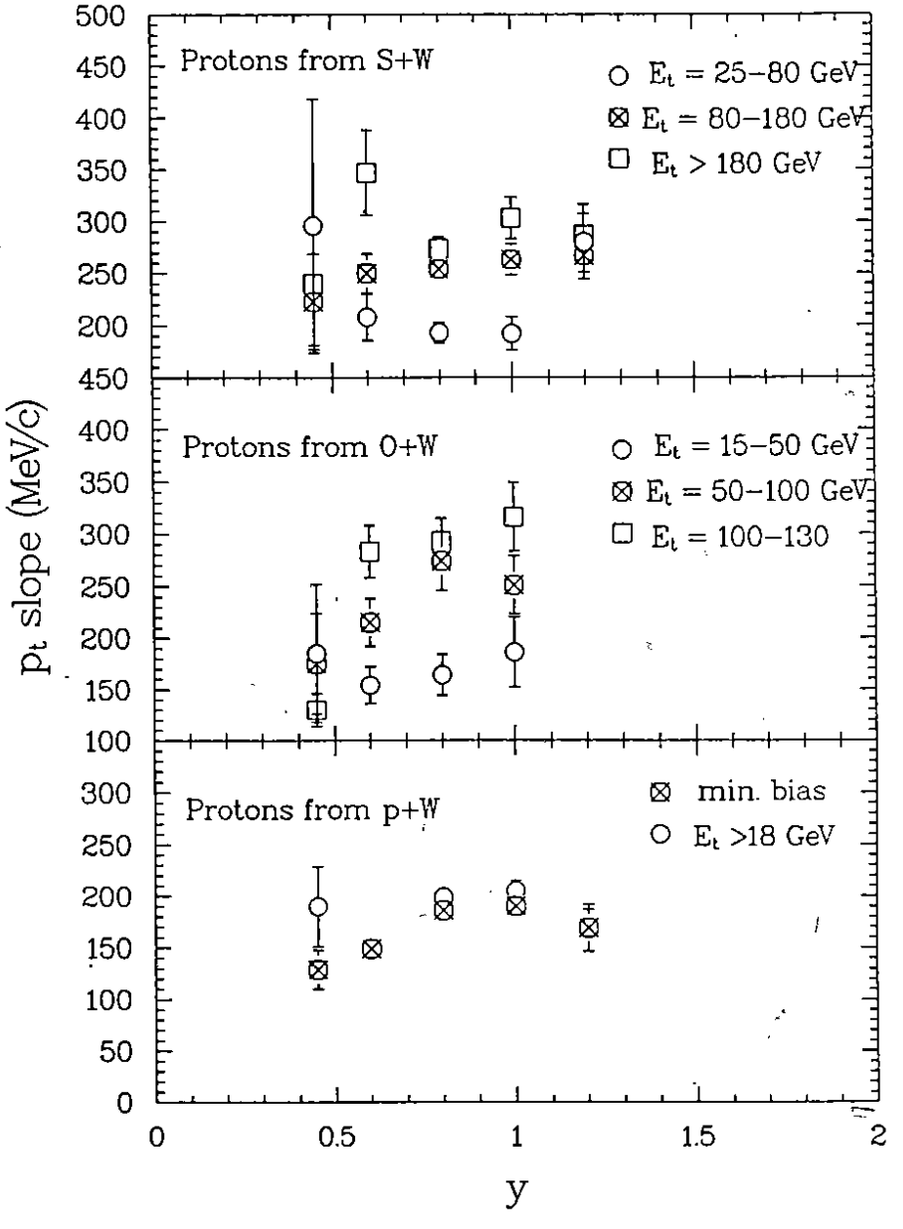
Protons from S+W
E_t = 25–80 GeV
E_t = 80–180 GeV
E_t > 180 GeV
Protons from O+W
E_t = 15–50 GeV
E_t = 50–100 GeV
E_t = 100–130
Protons from p+W
min. bias
E_t >18 GeV
p_t slope (MeV/c)
y

Fig. 10

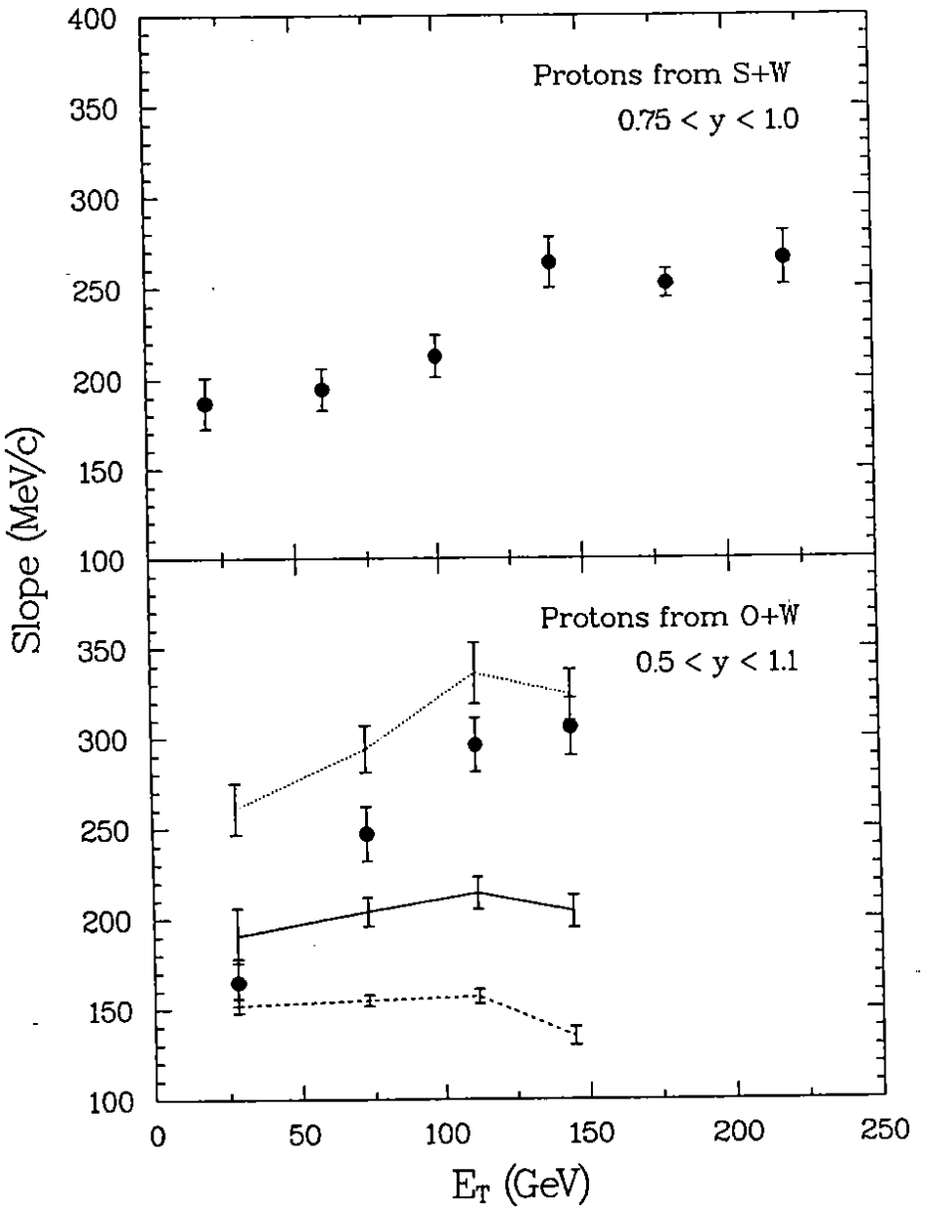

Fig. 11

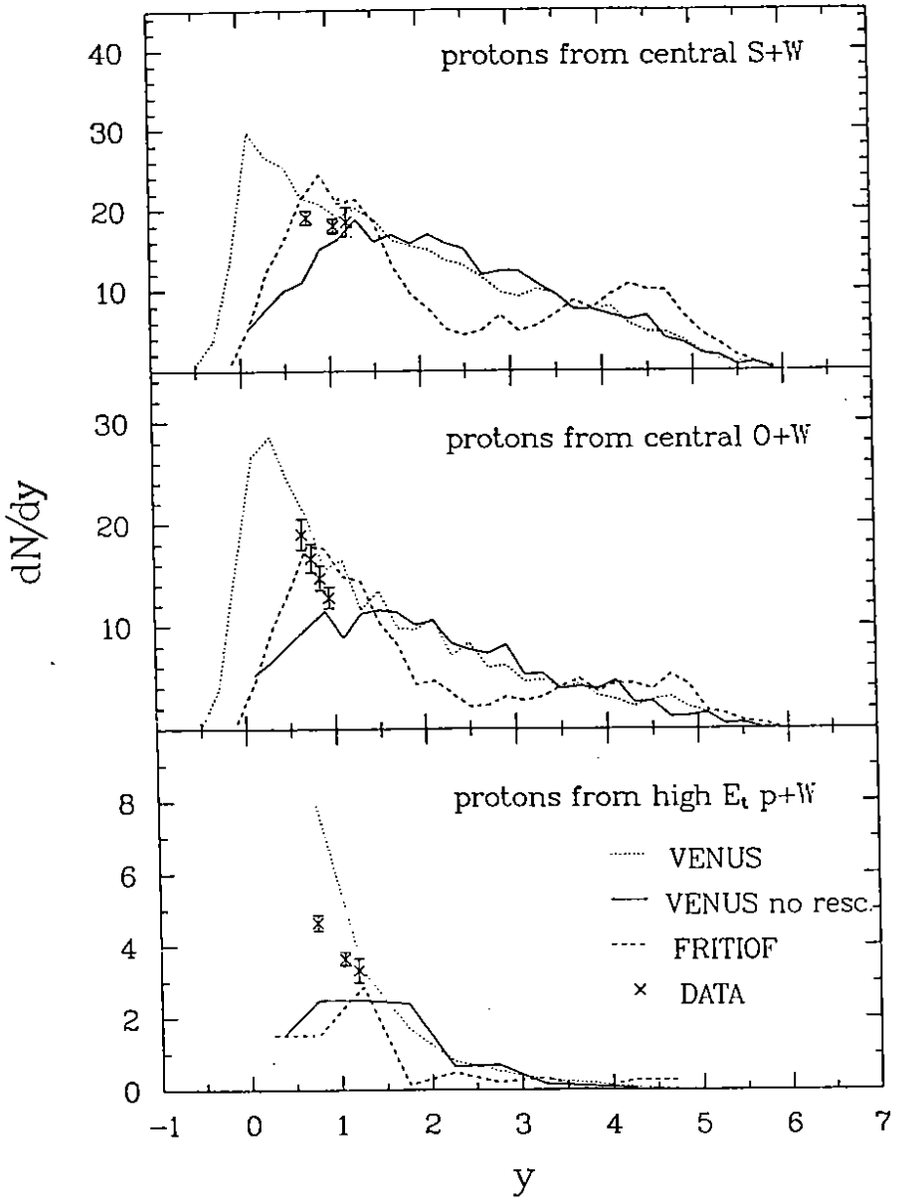

Fig. 12

Imprimé au CERN. Prix: 0.60 Fr.